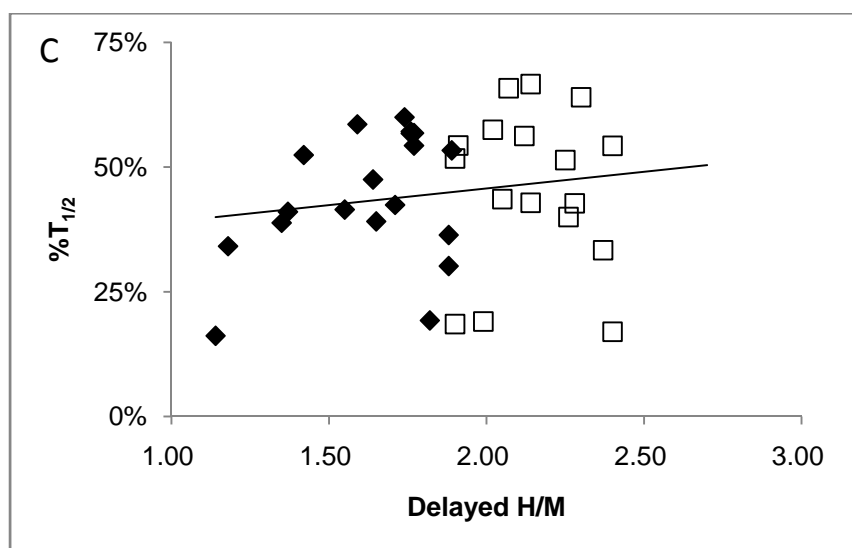
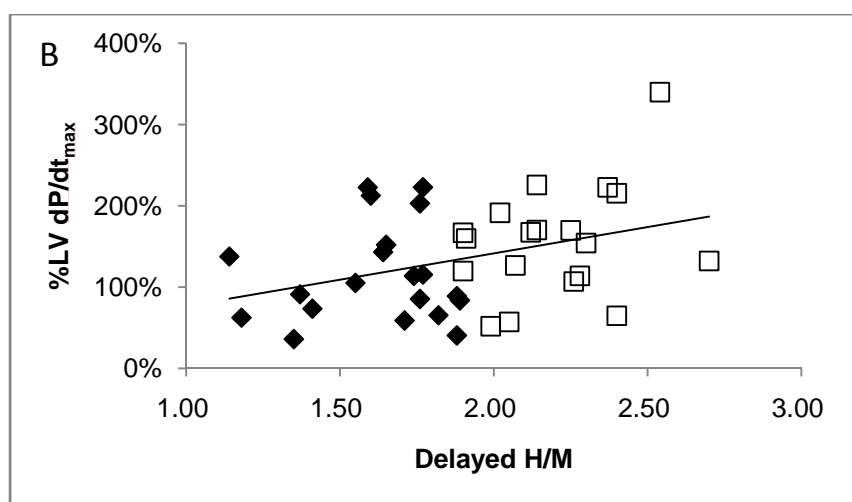
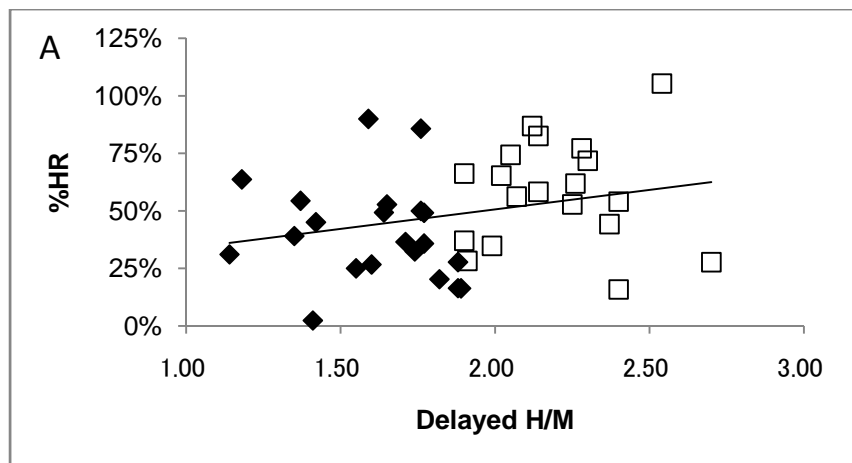
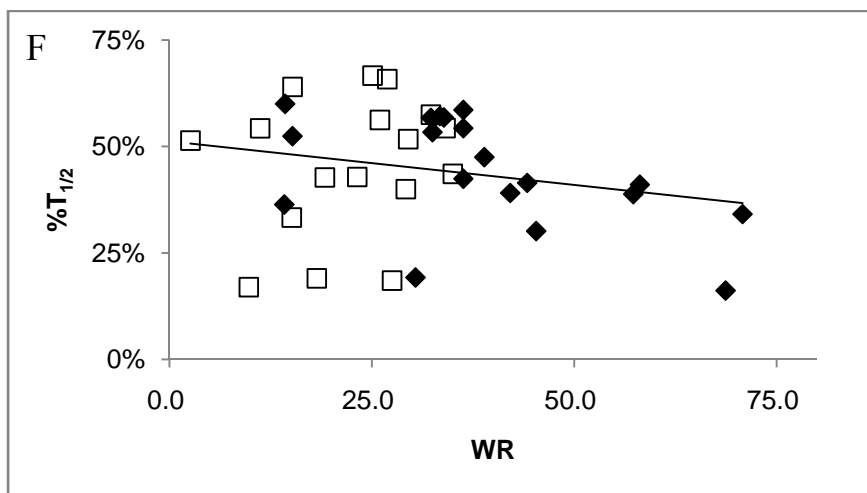
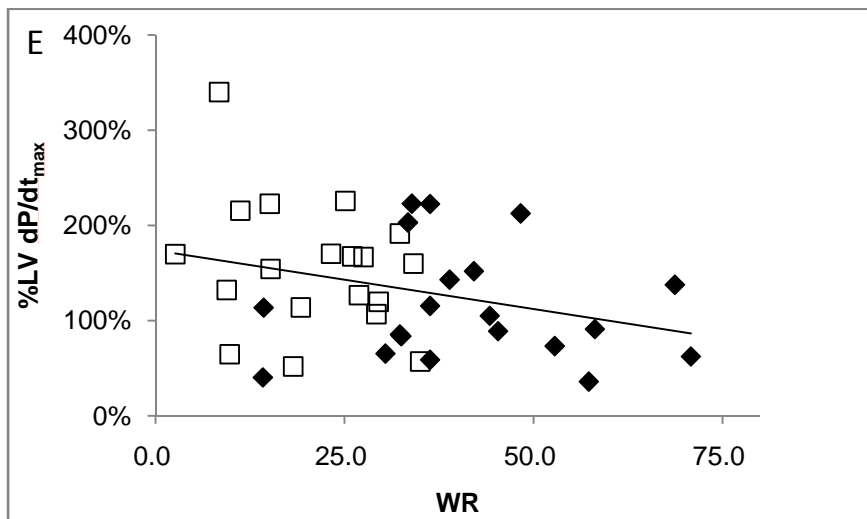
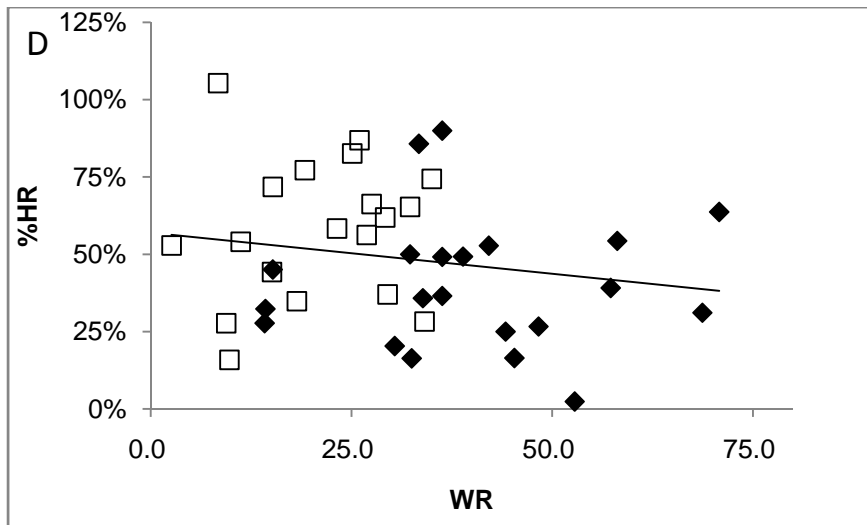
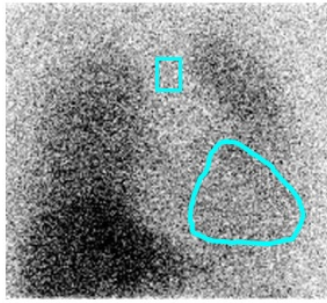


Figure 1

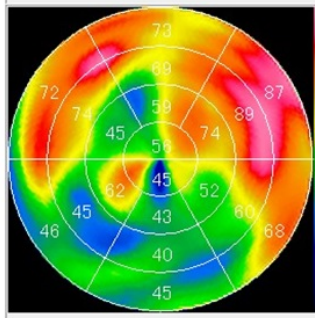




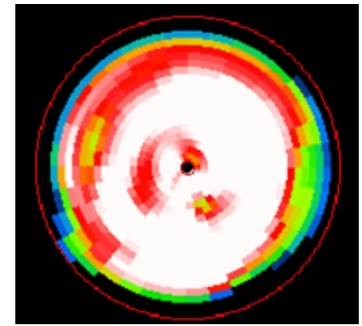
G



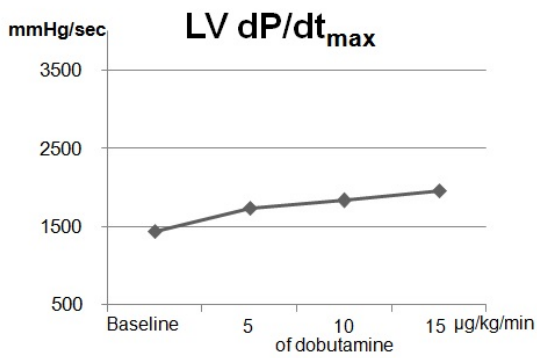
Planar



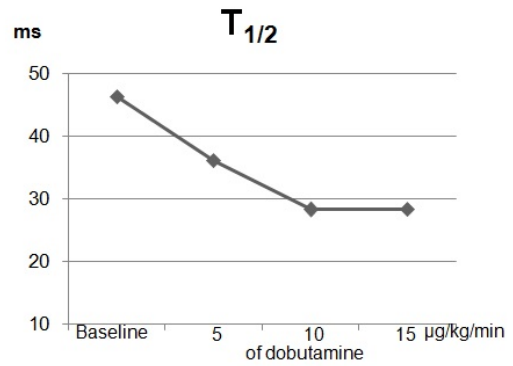
Myocardial distribution on delayed image



Washout map

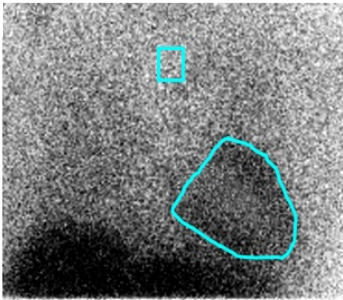


%LV dP/dt_{max}: 36 %

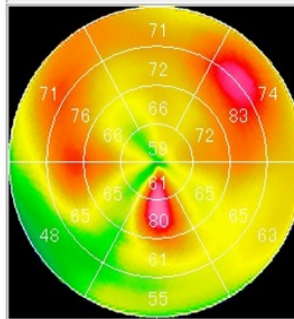


%T_{1/2}: 39 %

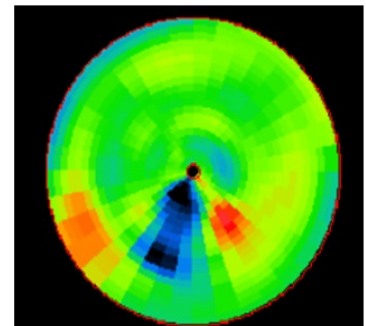
H



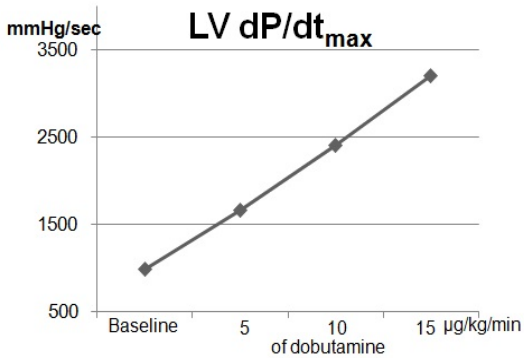
Planar



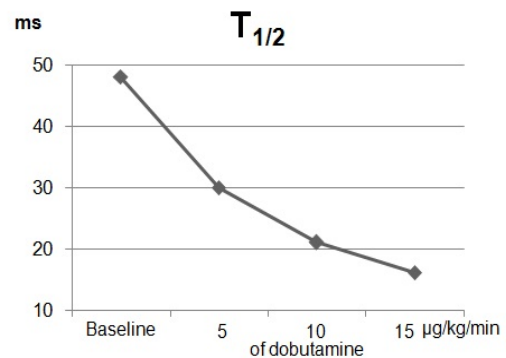
Myocardial distribution on delayed image



Washout map



%LV dP/dt_{max}: 226 %



%T_{1/2}: 67 %

Figure 1: ^{123}I -MIBG in DCM.

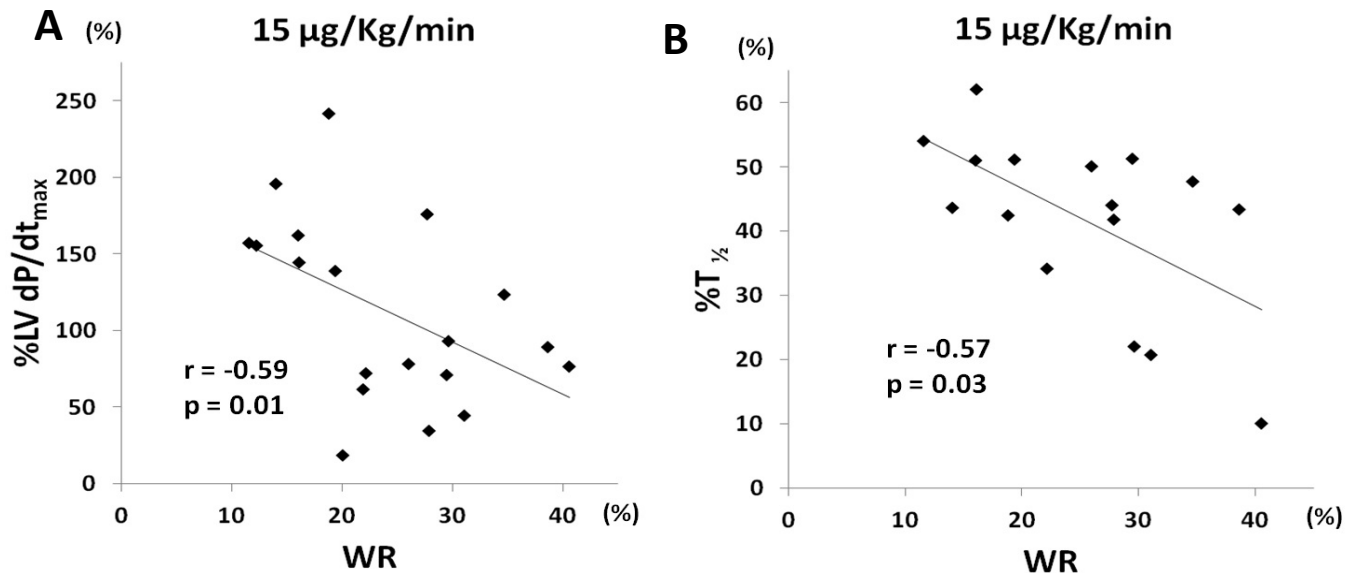
A-C. Relationships between delayed H/M of ^{123}I -MIBG and the parameters of cardiac catheterization. Significant correlations were observed between delayed H/M and % changes in HR(A), LV $\text{dP}/\text{dt}_{\text{max}}$ (B), and $T_{1/2}$ (C).

D-F. Relationships between washout rate of ^{123}I -MIBG and parameters of cardiac catheterization. Significant correlations were observed between washout rate and % changes in HR(D), LV $\text{dP}/\text{dt}_{\text{max}}$ (E), and $T_{1/2}$ (F).

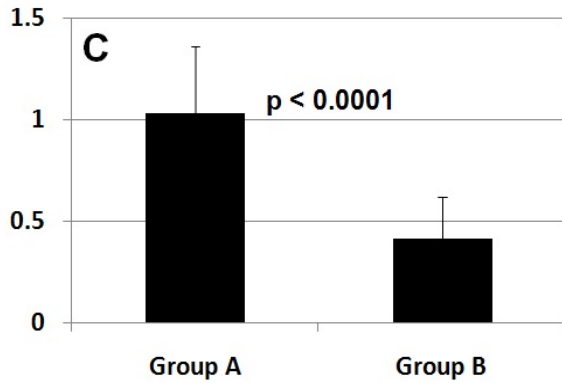
G. Representative Case of lower delayed H/M. A patient with markedly reduced cardiac uptake (delayed H/M = 1.5), globally increased washout of ^{123}I -MIBG shows impaired inotropic, chronotropic, and lusitropic responses to dobutamine stress.

H. Representative case of higher delayed H/M. A patient with preserved cardiac uptake (delayed H/M = 2.3) and only slight washout in the inferior wall of ^{123}I -MIBG shows a favorable change in HR and fair inotropic and lusitropic responses to dobutamine stress.

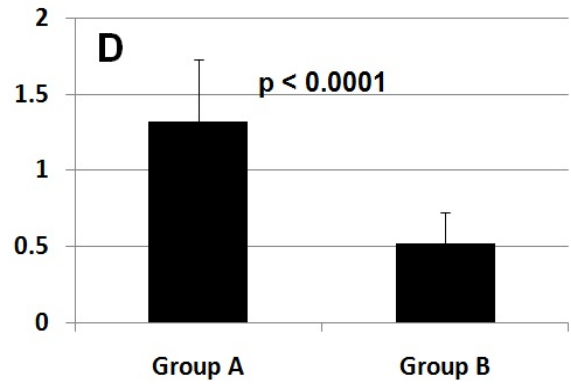
Figure 2



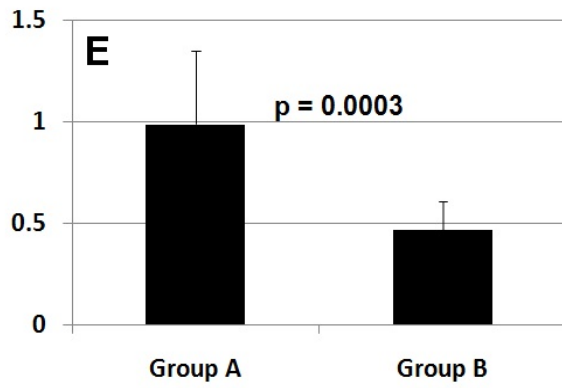
α-KGDH/GAPDH



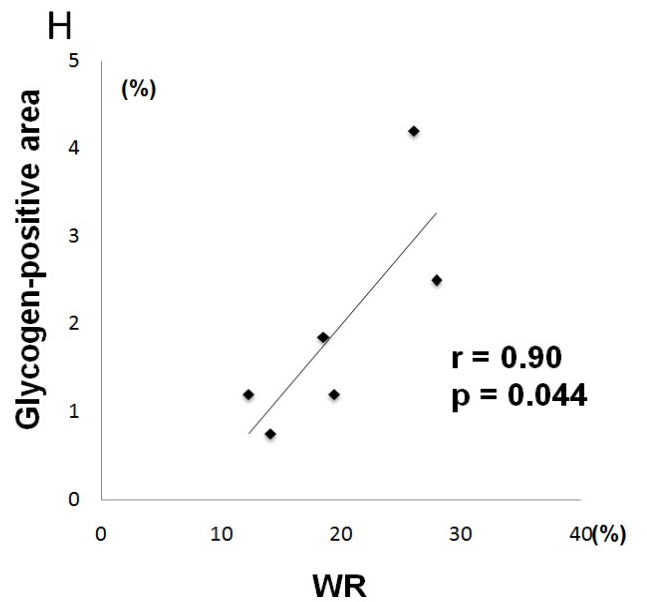
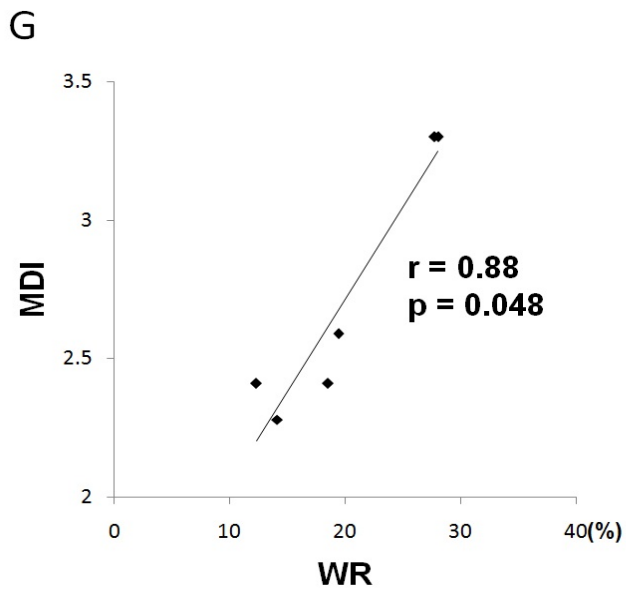
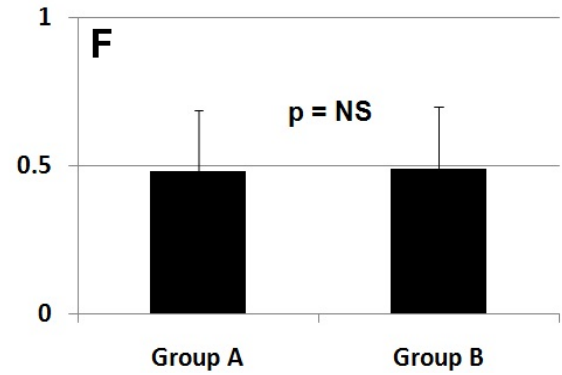
NDUFV3/GAPDH



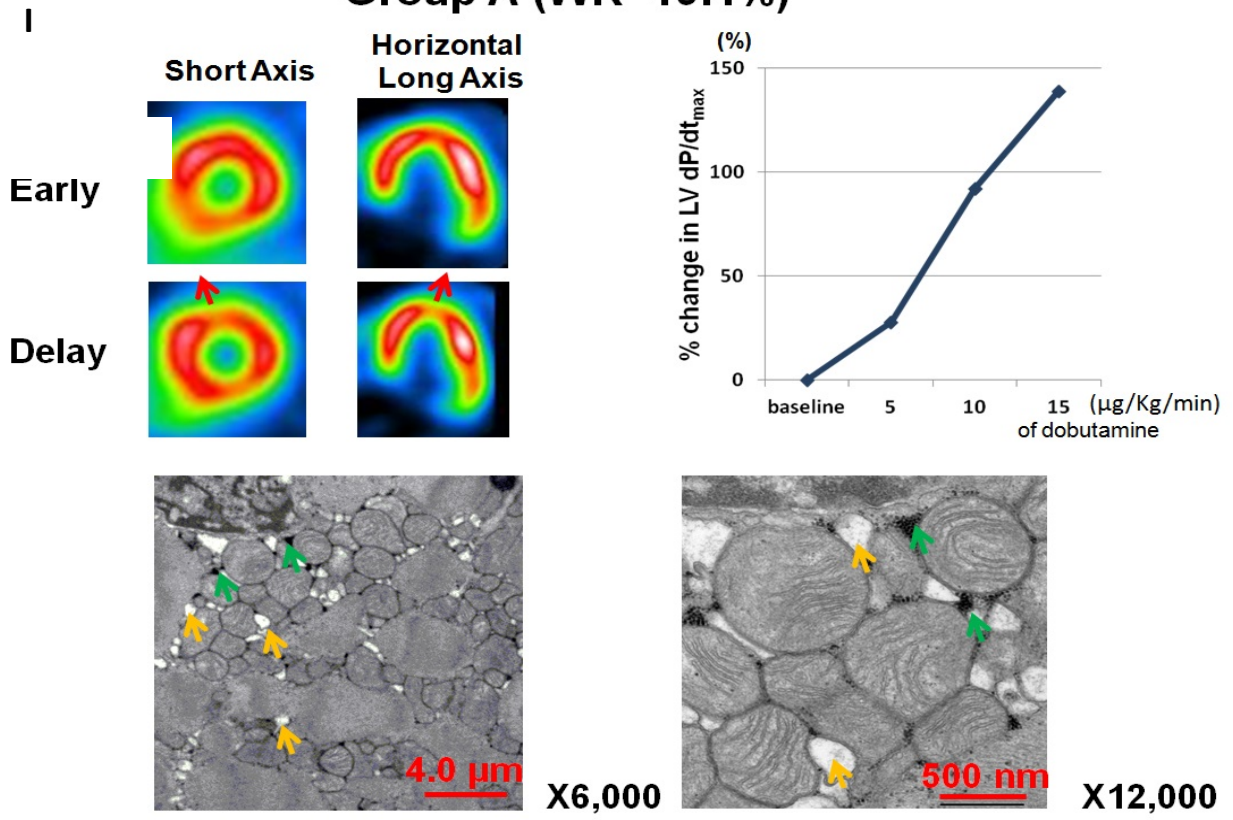
COX5B/GAPDH



P-Glycoprotein /GAPDH



Group A (WR=19.4%)



Group B (WR=28.0%)

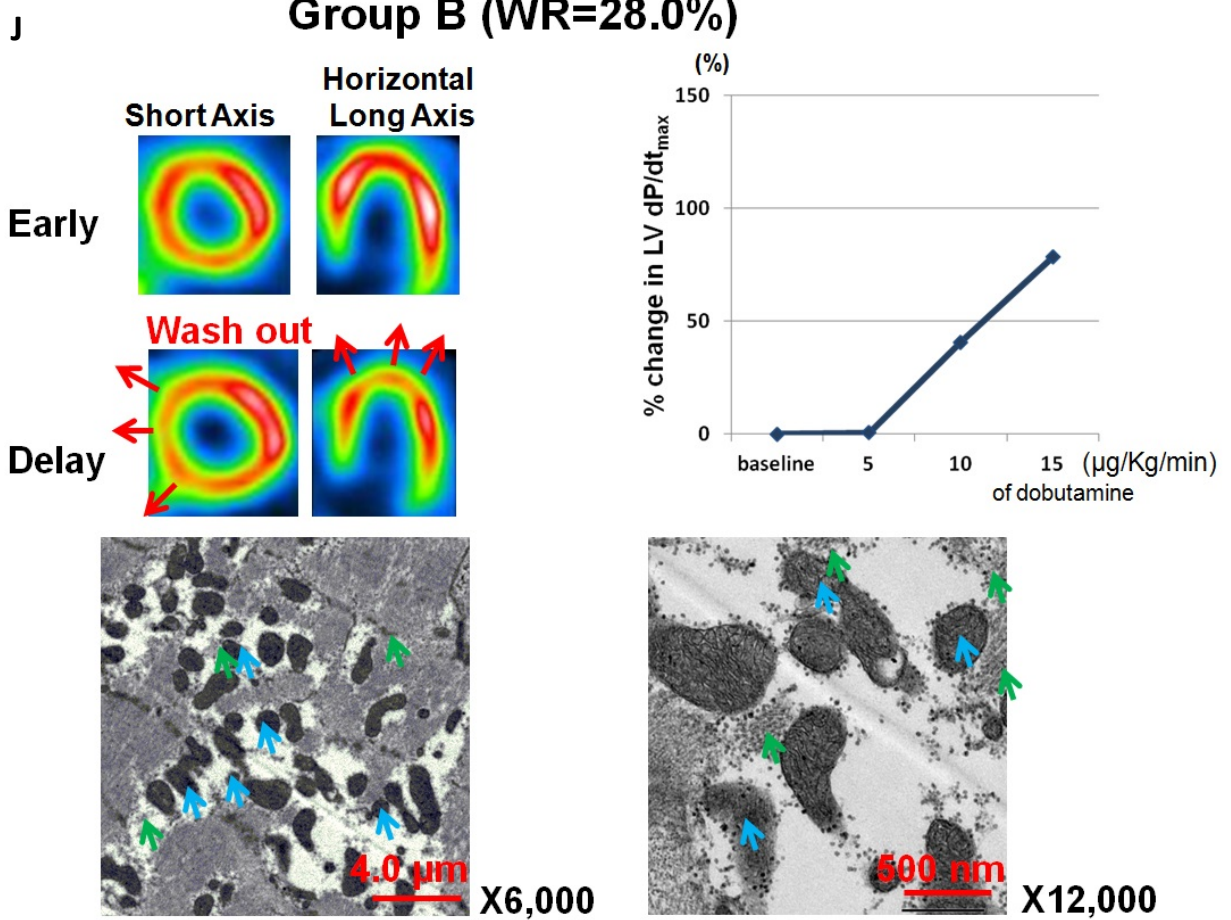


Figure 2: ^{99m}Tc -sestamibi in HCM

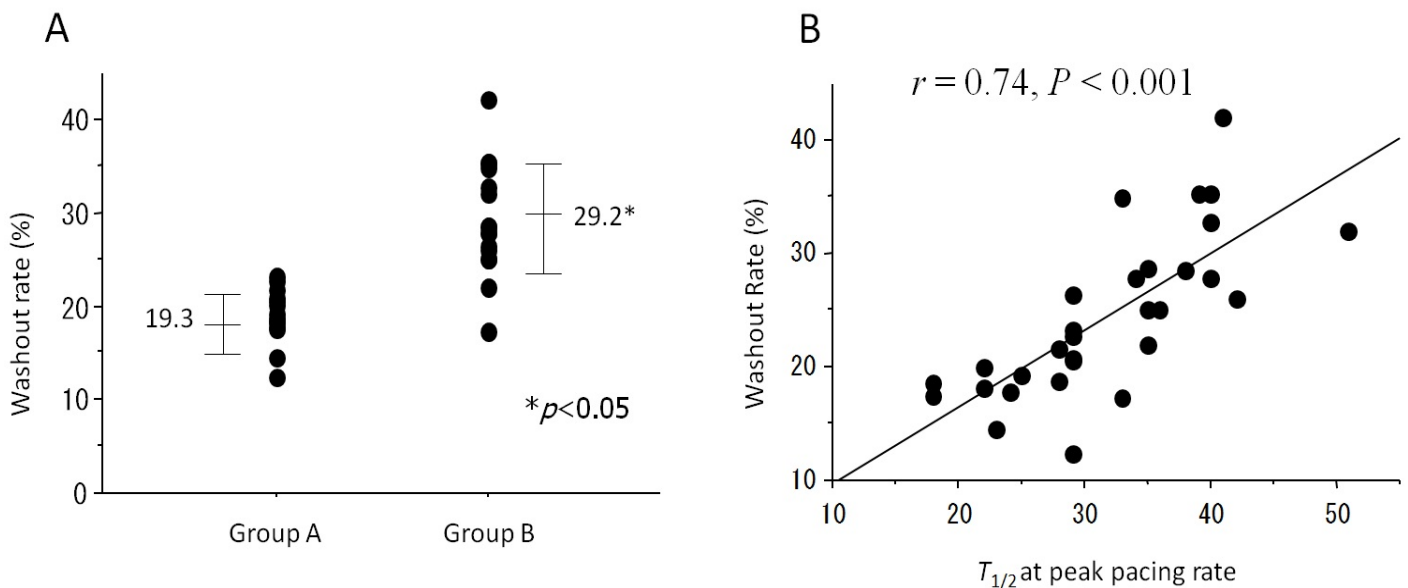
A, B. ^{99m}Tc -sestamibi washout rate for patients in groups A (normal force-frequency relations (FFR) and a pressure half time ($T_{1/2}$)) and B (abnormal FFR and $T_{1/2}$). A. Washout rate of Group B was significantly higher than that of Group A. B. Significant correlation between ^{99m}Tc -sestamibi washout rate and the $T_{1/2}$ at the peak pacing rate for all patients was observed.

C-E. Relation between ^{99m}Tc -sestamibi washout rate and the ventricular abundance of mitochondrial protein mRNAs. C. ^{99m}Tc -sestamibi washout rate and the α -ketoglutarate dehydrogenase (α -KGDH)/glyceraldehyde-3-phosphate dehydrogenase (GAPDH) mRNA ratio. D. ^{99m}Tc -sestamibi washout rate and the nicotinamide adenine dinucleotide dehydrogenase flavoprotein 3 (NDUFV3)/GAPDH mRNA ratio. E. ^{99m}Tc -sestamibi washout rate and the cytochrome c oxidase subunit 5B (COX5B)/GAPDH mRNA ratio.

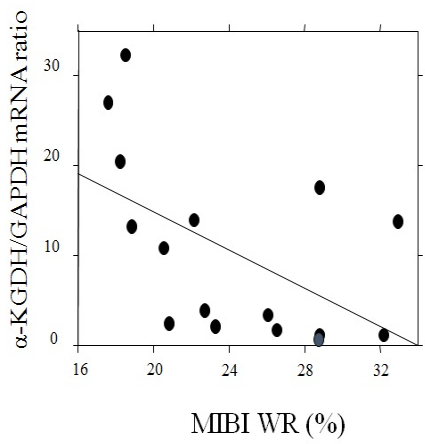
F, G. Representative electron micrographs of ventricular sections from patients in Group A (F) and Group B (G). H. The size variation of mitochondria in group B was significantly greater than that in group A. I. Distance from the centre of each mitochondrion to the nearest myofibril in Group B was significantly greater than that in group A.

J, K. Representative FFR and scintigraphic findings for patients in Groups A (J) and B (K). J. The relation between heart rate and the % change in LV $\text{dP}/\text{dt}_{\text{max}}$ during atrial pacing of a patient in Group A shows a progressive increase in LV $\text{dP}/\text{dt}_{\text{max}}$ with heart rate (relatively normal response) (left panel). The ^{99m}Tc -sestamibi SPECT images for this patient appear normal (right panel). K. The patient of Group B shows a biphasic force–frequency relation (left panel). The patient shows mildly reduced uptake in the septum on the early images (right panel), and increased ^{99m}Tc -sestamibi washout, especially at the septal wall (arrow heads in the right panel).

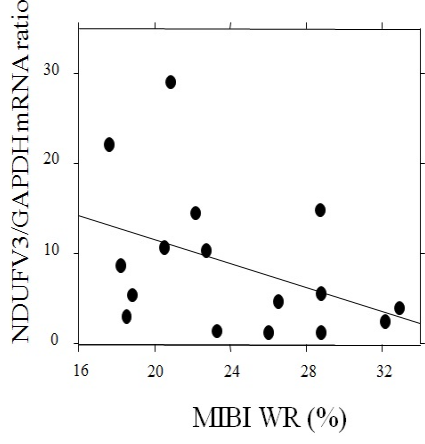
Figure 3



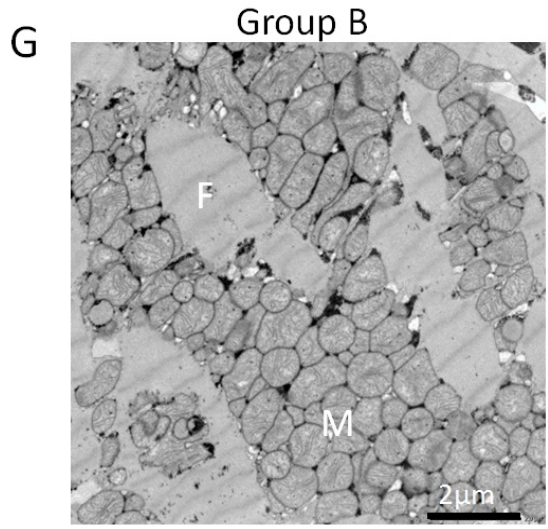
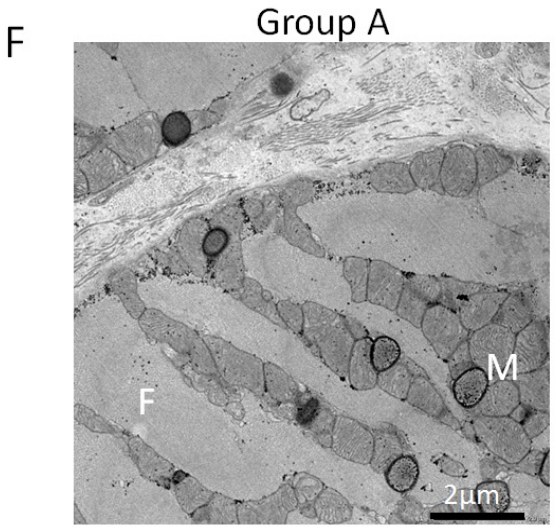
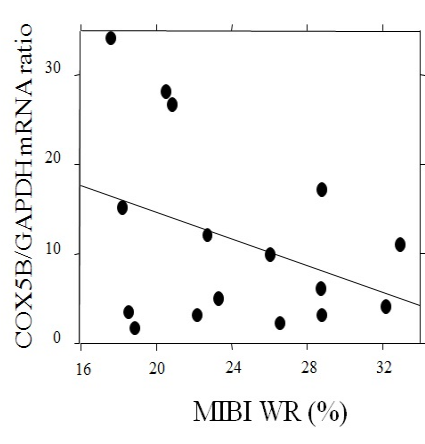
C $r = -0.53, P < 0.05$



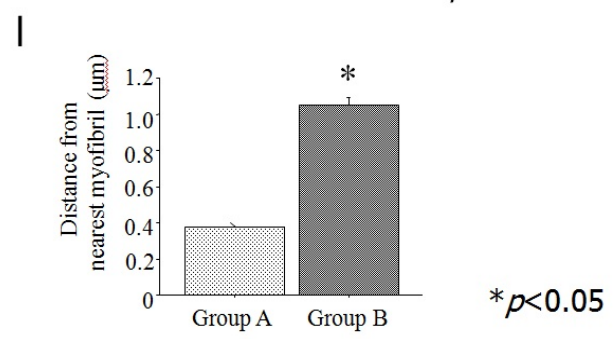
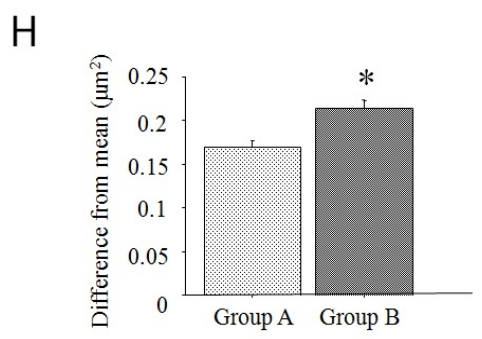
D $r = -0.42, P = 0.10$



E $r = -0.37, P = 0.16$



M: mitochondria F: myofibril



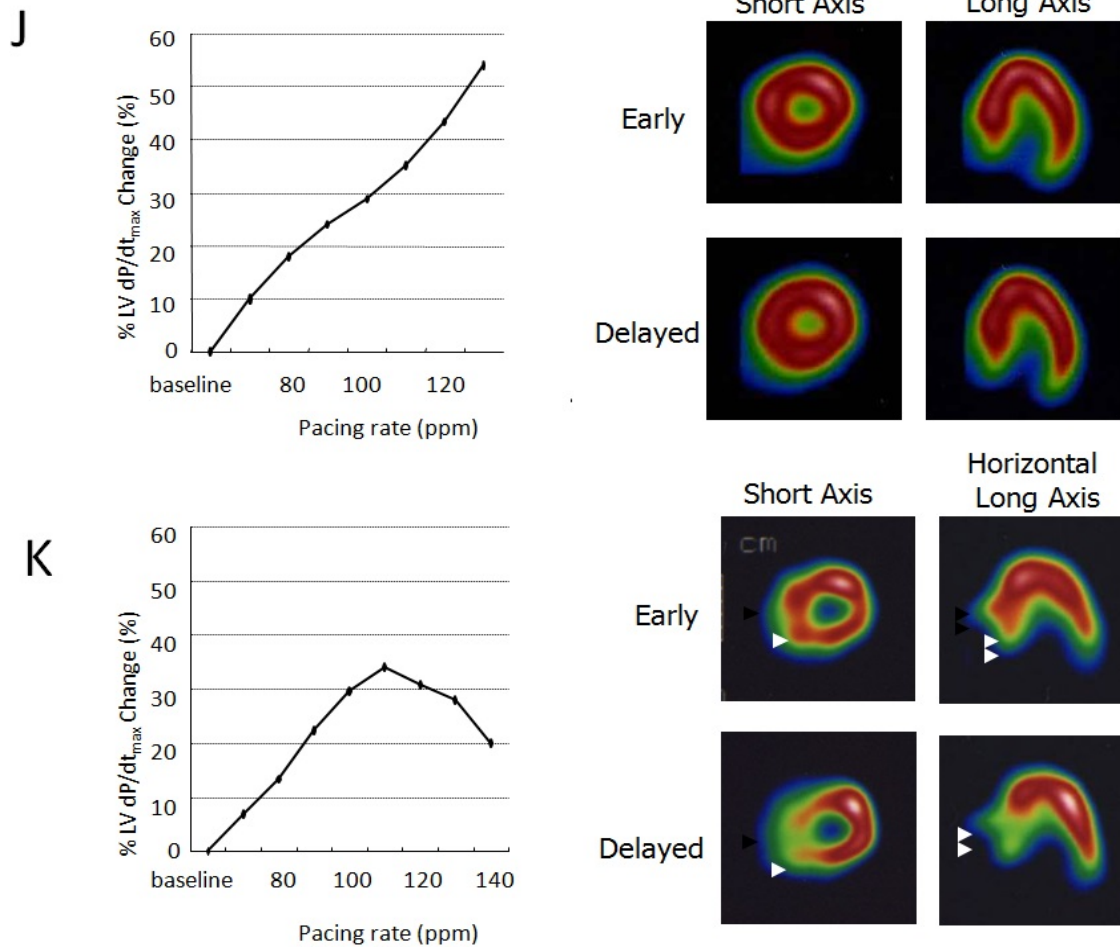


Figure 3: ^{99m}Tc -sestamibi in DCM.

A, B. Relationship between ^{99m}Tc -sestamibi washout rate (WR) and hemodynamic changes from baseline to peak dobutamine stress. A. A significant inverse correlation was observed between ^{99m}Tc -sestamibi WR and % changes in LV dP/dt_{\max} from baseline to peak (15 $\mu\text{g}/\text{kg}/\text{min}$) dobutamine stress. B. A significant inverse correlation was observed between ^{99m}Tc -sestamibi WR and % changes in $T_{1/2}$ from baseline to peak (15 $\mu\text{g}/\text{kg}/\text{min}$) dobutamine stress.

C-F. Comparison of mitochondrial mRNA expression between the 2 Groups. α -KGDH (C), NDUFV3 (D), and COX5B (E) were significantly lower in Group B (WR of ^{99m}Tc -sestamibi $\leq 24.3\%$) than in Group A (WR of ^{99m}Tc -sestamibi $> 24.3\%$).

G, H. Relationship between ^{99m}Tc -sestamibi WR and parameters of electron microscopic findings. Significant correlations were observed between ^{99m}Tc -sestamibi WR and the mitochondria damage index (G) and glycogen-positive areas (H).

I. Representative Case of group A. A 66-year-old man shows no global increased ^{99m}Tc -sestamibi WR (19.4%). An increased washout was observed in the small anteroseptal area (red arrows) on SPECT image. The % % change in LV dP/dt_{\max} was favorably increased. Electronmicroscopy revealed a

relatively preserved mitochondrial configuration as well as a small amount of glycogen accumulations (green arrows) and lipid droplets (yellow arrows).

J. Representative case of group B. A 45-year-old woman exhibited an increased ^{99m}Tc -sestamibi WR (28.3 %). An increased washout was observed in the anteroseptal to the inferoseptal wall. The % change in LV dP/dt_{max} showed a subtle increase in response to dobutamine. Electron microscopy reveals many damaged mitochondria (blue arrows) and glycogen accumulations (green arrows).

Figure 4

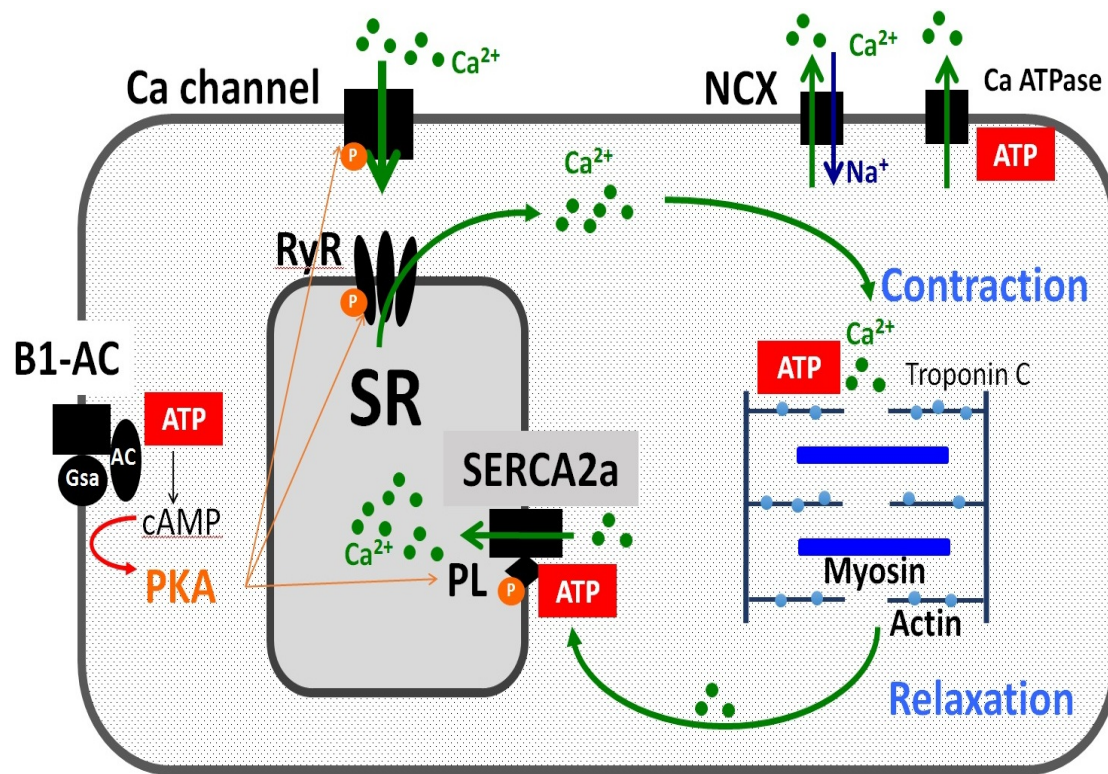


Figure 4: Calcium handling related protein is impaired in the failing heart. Calcium influx through cell membrane calcium channel induces calcium-induced calcium release from sarcoplasmic reticulum (SR) through ryanosine receptor (RyR). Then, intra-cellular calcium binding to the actin filament induces the sliding of the actin-myosin filament, resulting in myocardial contraction. Calcium dissociation from actin filament cause myocardial relaxation, and calcium is retaken up to SR through sarcoplasmic reticulum calcium ATPase (SERCA2a), regulated by phospholamban (PL). Intracellular calcium concentration is regulated with a calcium pump out trough natrium calcium exchanger or plasma membrane calcium ATPase. Beta adrenal stimulus activates phosphokinase A, which makes for phosphorylation of calcium

channel, RyR, PL, and the calcium handling cycle is activated. Each process consumes an amount of ATP, and the lack of ATP would have a harmful effect on calcium handling and reduced cardiac function. NCX: Na⁺/Ca²⁺ exchanger; SR: sarcoplasmic reticulum; SERCA2a: sarcoplasmic reticulum Ca²⁺ ATPase; PL: phospholamban; PKA: phosphokinase A; CAMP: cyclic AMP; AC: adenylate cyclase; RyR: Ryanosine receptor; B1-AR: beta1 adrenal-receptor.

Table 1: Molecular imaging of the failing heart.

Target	Tracer
Energy substrate Glucose	¹⁸ F-FDG
Free fatty acid	¹²³ I-BMIPP
Oxidative metabolism	¹¹ C-acetate
Mitochondria	^{99m} Tc-sestamibi
Sympathetic Nerve	¹²³ I-MIBG
Inflammation	¹⁸ F-FDG (fasting)